Relating the $4s\sigma^{-1}$ inner-valence photoelectron spectrum of HBr with the Br $3d^{-1}5l\lambda$ resonant Auger spectra: An approach to the assignments

R. Püttner,[1] Y. F. Hu,[2] G. M. Bancroft,[2] A. Kivimäki,[3] M. Jurvansuu,[3] H. Aksela,[3] and S. Aksela[3]
[1]*Institute for Experimental Physics, Freie Universität Berlin, Arnimallee 14, D-14195 Berlin, Germany*
[2]*Department of Chemistry, The University of Western Ontario, London, Ontario, Canada N6A 5B7*
[3]*Department of Physical Sciences, University of Oulu, P.O. Box 3000, 90401 Oulu, Finland*
(Received 28 May 2003; published 10 September 2003)

The high resolution Br $4s\sigma^{-1}$ photoelectron spectrum of HBr is presented together with the resonant Auger spectra resulting from excitations from the $3d$ core levels to the low-n Rydberg orbitals $5s\sigma$, $5p\sigma$, and $5p\pi$. The very complex spectra can be broadly assigned using two observations. First, the energy splittings of the $4p\pi^{-2}5s$ and $4p\pi^{-2}5p$ states are very similar to the splittings of the $4p\pi^{-2}(^1\Sigma^+, ^1\Delta,$ and $^3\Sigma^-)$ final states seen previously in the normal Auger spectra. Second, the $^2\Sigma^+$ states, which are the dominant correlation satellites in the complex $4s\sigma^{-1}$ photoelectron spectrum, are often enhanced in the $5s\sigma$ resonance Auger spectra. Electron correlation and spin-orbit interaction in the final states are important to understand all of these spectra. Unlike the normal Auger spectra, vibrational excitations play only a minor role in these spectra, showing that the $5s$ and $5p$ Rydberg orbitals have some bonding character.

DOI: 10.1103/PhysRevA.68.032705 PACS number(s): 32.80.Hd, 33.80.Eh

I. INTRODUCTION

In the last few years, there have been many high-resolution resonant Auger studies of rare gas atoms and diatomic molecules [1–3]. As expected for resonant Auger spectra, the total spectral linewidths were much narrower than those limited by the core-hole lifetime, and the lines disperse with the photon energy. The atomic spectra have revealed incredibly rich detail (for example, over 350 lines have been resolved in the Kr $3d^{-1}np \rightarrow 4p^{-2}nl$ resonance Auger spectra), and high-quality calculations have been necessary to interpret these spectra [4,5]. The majority of the molecular spectra have involved core to antibonding transitions (for example, in HBr [6], HCl [7], CO [8], CO_2 [9], NO [10], and H_2O [11]), and these studies focused on molecular dissociation and vibrational interference effects. To our knowledge, there have been only a few studies of resonant Auger spectra in molecules subsequent to core-to-Rydberg excitations (for example, in CO [12–15], HCl [16,17], and HBr [18]).

The resonant Auger spectra of HCl and HBr [16–18] are still not well understood, and will eventually require high-quality calculations to fully interpret them. In our preliminary report on resonant Auger spectra dealing with a few of the Br $3d^{-1}$ to Rydberg transitions [18], we used these spectra to interpret the Br $3d$ photoabsorption spectrum [19–22], which was also not fully understood. However, without a detailed understanding of the photoabsorption spectrum, it is considerably more difficult to interpret the resonant Auger spectra, in particular if it is not known whether the spectator electron is $5s$, $4d$, $5p\sigma$, $5p\pi$, or a higher-ns,p, or d Rydberg electron. Our preliminary resonant Auger study of HBr [18] was very useful in pinpointing the $5p\pi$ and $5p\sigma$ energies; but the lowest-energy Rydberg orbital was thought to be the $4d\pi$ at the time, and this assignment was in contradiction to the lines observed in the resonant Auger spectra of the excitations into this orbital. Subsequently, we have refined the interpretation of both the HBr Br $3d$ photoabsorption spectrum [23] and the Br MVV Auger spectrum [24], and we now consider that the interpretation of both these spectra is quantitative. For example, using angle-resolved photoabsorption spectra of HBr, we have shown that the lowest-energy Rydberg line in the Br $3d$ spectrum must be assigned to a transition to the $5s\sigma$ orbital and not the $4d\pi$ orbital [23]. The interpretation of the equally complex Auger spectrum required a detailed knowledge of vibrational and ligand field effects as well as vibrational lifetime interference [24]. The splitting energies of the $4p^{-2}$ hole states obtained from the normal Auger studies of HBr are incredibly important for the interpretation of spectra that involve $4p^{-2}nl\lambda$ spectator states in both the Br $4s\sigma^{-1}$ photoelectron and the resonant Auger spectra of the $3d^{-1}nl\lambda$ resonances.

Although not many details are known about the Br $4s\sigma^{-1}$ photoelectron spectrum of HBr, this spectrum is important for understanding the resonant Auger spectra since some of the final states of the resonant Auger process have the same symmetry ($^2\Sigma^+$) and similar binding energies as the Br $4s\sigma^{-1}$ configuration and can, therefore, mix with this configuration. From literature it is known that a strong mixing between the different configurations actually occurs in the inner-valence region of HCl [25] and HBr [26]. This can be observed in the $3s\sigma^{-1}$ and $4s\sigma^{-1}$ photoelectron spectra of HCl and HBr, respectively, which both reveal a very rich structure. In recent years some publications focused on the Cl $3s\sigma^{-1}$ photoelectron spectrum of HCl, enlightening some of the effects present in that spectrum. However, the entire complexity of the spectrum becomes obvious by the fact that two very recent adjoint publications [27,28] deal only with effects present in the main line of the Cl $3s\sigma^{-1}$ photoelectron spectrum. The recent high-resolution Kr $4s$ spectrum [29,30] with over 100 resolved lines gives another example of the great complexity of this kind of spectrum resulting from a myriad of different electronic states. Up to now, no high-resolution $4s$ photoelectron spectrum of HBr has been

published, but the low-resolution photoelectron spectrum [31] and a high-resolution threshold photoelectron spectrum [26] show great challenges to interpret these spectra of even the simplest diatomic molecules.

Recently, some studies on the resonant Auger decay of the Cl $2p^{-1}4s$, $4p$, and $3d$ resonances in HCl have been reported [16,17] and the main features of these spectra were assigned. Due to the similarity in the valence electron structures of HBr and HCl, similar final-state configurations are expected, namely, $mp\pi^{-2}nl\lambda$ with m being 3 for HCl and 4 for HBr. However, due to the considerably heavier Br nucleus as compared to the Cl nucleus, a stronger spin-orbit interaction is expected in HBr resulting in a mixing of states with different $\Sigma\Lambda$ symmetry. A similar mixing of states with different LS symmetry has been observed in the $4s^{-1}$ photoelectron spectrum of krypton [30], which is isoelectronic to HBr.

In the present study, we present high-intensity, high-resolution (total linewidth of about 30 meV) Br $4s\sigma^{-1}$ photoelectron spectrum, and the resonant Auger spectra (total linewidth of 30 meV) resulting from excitation of the Br $3d$ level to low Rydberg states, such as $5s\sigma$, $5p\pi$, and $5p\sigma$ Rydberg orbitals. By relating these spectra to each other, we are able to assign most of the lines in these spectra to different symmetry states with small vibrational components without support of theoretical predictions. Fortunately, vibrational effects are very small in these resonant Auger spectra as well as in the $3d$ photoabsorption and photoelectron spectra [32]; these facts make the assignment less difficult, in particular, since we do not have to take vibrational substates of the intermediate state into account.

II. EXPERIMENT AND DATA ANALYSIS

The electron spectra of HBr were measured using beamline I411 at the 1.5-GeV storage ring MAX II in Lund, Sweden. The beamline, using synchrotron radiation from a hybrid undulator with 44.5 periods and a 58.8-mm period length, provides photons from 50–1200 eV using a Zeiss SX-700 plane grating monochromator. Photon resolution at 80 eV using exit slit width of 20 μm was about 10 meV which was required to excite transitions selectively. The electron spectra were collected at an angle of 54.7° with respect to the electric-field vector of light (magic angle) using a high-resolution Scienta SES 200 hemispherical electron analyzer, and a total linewidth of 20 meV on the Kr $4p^{-1}$ and $4s^{-1}$ photoelectron lines was obtained at 56 eV photon energy with 10 eV pass energy and 30 meV with 20 eV pass energy used for the Br $4s^{-1}$ photoelectron and resonant Auger spectra of HBr. Commercial HBr was introduced into the gas cell equipped with a differential pumping system.

For the Br $4s\sigma^{-1}$ photoelectron spectrum a least-squares fit analysis was performed in order to obtain binding energies and relative intensities, in particular for the narrow lines. In this fit analysis all lines were described by pure Gaussian profiles. This approach is also reasonable for the narrow lines since the natural widths of these lines are expected to be much smaller than the total experimental resolution caused by photon resolution and the spectrometer resolution. The electron binding energies are accurate to better than 10 meV.

The purpose for the fit analysis of the Br $4s\sigma^{-1}$ photoelectron spectrum was to provide relative intensities for the narrow lines which can be compared with future theoretical results. A similar analysis for the resonant Auger spectra was not performed, since it turned out that the relative intensities partly depend on the excitation energy (see below).

III. THE $4s\sigma^{-1}$ PHOTOELECTRON SPECTRUM AND THE RESONANT AUGER SPECTRA AT THE $3d^{-1}5s\sigma$ RESONANCES

The main lines of the $4s\sigma^{-1}$ photoelectron spectrum and the resonant Auger decay spectrum taken at the $3d^{-1}5s$ resonances overlap strongly. During the data analysis of these spectra, it was realized that the understanding of the $4s\sigma^{-1}$ photoelectron spectrum is important to understand the resonant Auger spectrum and vice versa. In particular, the resonant Auger spectrum recorded at the $3d^{-1}5s\sigma$ resonances show only five extra lines (out of over 40 lines) in addition to those of the $4s\sigma^{-1}$ photoelectron spectrum. Therefore, in the present section both spectra are presented and discussed together.

A. The $4s\sigma^{-1}$ photoelectron spectrum of HBr

In the ground state the valence shell of HBr can be described with the configuration $(7\sigma)^2(8\sigma)^2(4\pi)^4(9\sigma)^0$ with contributions from the configuration $(7\sigma)^2(8\sigma)^0(4\pi)^4(9\sigma)^2$ for larger bond distances in order to describe the ionic dissociation of the molecule correctly [33]. 7σ,8σ,4π, and 9σ represent the Br $4s\sigma$, the bonding Br $4p\sigma-$ H $1s$, the nonbonding Br $4p\pi$, and the antibonding Br $4p\sigma-$ H $1s$ orbitals, respectively. By neglecting the ground-state configuration interaction, i.e., the contributions of the configuration $(7\sigma)^2(8\sigma)^0(4\pi)^4(9\sigma)^2$, the Br $4s\sigma^{-1}$ ionization is the only one that carries intensity in the binding-energy range around 25 eV and leads to an ionic state with $^2\Sigma^+$ symmetry. By assuming predominantly LS coupling we can conclude that the intense correlation satellites observed in the photoelectron spectrum have predominantly $^2\Sigma^+$ symmetry as well. This effect will be utilized to understand the Br $4s\sigma^{-1}$ photoelectron spectrum, together with a comparison of the Br $4s\sigma^{-1}$ photoelectron spectrum with the Br $3d^{-1}5s\sigma$ resonant Auger spectra.

Figure 1 displays an overview of the Br $4s\sigma^{-1}$ photoelectron spectrum of HBr, and Table I summarizes the peak energies, relative intensities, and assignments of the lines. The spectrum consists of eight groups of lines which are due to strong electron correlation and are labeled A to H. Four groups of lines (A, B, E, and H) are mainly broad and without fine structure. These lines are due to transitions to the $2h$-$1p$ molecular configurations, which are dissociative, such as $4p\pi^{-2}\sigma^*$, $4p\pi^{-1}\,4p\sigma^{-1}\sigma^*$, $4p\pi^{-1}\,4p\sigma^{-1}nl\lambda$, $4p\sigma^{-2}\sigma^*$, and $4p\sigma^{-2}nl\lambda$. Groups C, D, F, and G show a number of very narrow lines; these are due to transitions to the $4p\pi^{-2}nl\lambda$ configurations, which are stable with respect to dissociation. Groups A and B also overlap with some weak

but narrow lines which are assigned to transitions to the $4p\pi^{-2}nl\lambda$ configurations.

In particular, the most intense peak *B* can be assigned to the $4s\sigma^{-1}$ configuration interacting with a dissociative $2h$-$1p$ configuration which experience an avoided crossing in the Franck-Condon region. The strong contribution of the $4s\sigma^{-1}$ configuration gives rise to the intensity, while the avoided crossing with the $2h$-$1p$ configuration leads to a dissociative potential curve and, therefore, the broad peak. The narrow structures on peak *B* can probably be understood in an analogous way to very recent results obtained for the Cl $3s\sigma^{-1}$ photoelectron spectrum of HCl [27,28]. In these publications narrow Fano-like line shapes were reported on the top of the main line of the Cl $3s\sigma^{-1}$ photoelectron spectrum. However, based on the signal-to-noise ratio and the experimental resolution of the present $4s\sigma^{-1}$ photoelectron spectrum we can neither support nor reject a similar observation on the top of line *B* for HBr.

The broad part of line *A* can be assigned to excitations to the dissociative potential curve mainly due to the configuration $4p\pi^{-2}(^1\Sigma^+)\sigma^*(^2\Sigma^+)$. This assignment has been suggested by Yencha *et al.* [26] based on calculations performed by Banichevich *et al.* [34]. The broad line *E* is tentatively assigned to transitions to the states $4p\sigma^{-1}4p\pi^{-1}(^{3,1}\Pi)5p\pi(^2\Sigma^+)$ (see below). In the energy range of the narrow lines labeled A_1 to A_6, *B*, and C_1 to C_7, Yencha *et al.* [26] also found a large number of transitions to the final ionic states including a vibrational progression by using threshold photoelectron spectroscopy. However, due to the lack of precise theoretical calculations in this energy region they were not able to present a detailed assignment.

The final states of the most intense satellites in the $4s^{-1}$ photoelectron spectrum of krypton are $4p^{-2}(^1D)5d(^2S)$ and $4p^{-2}(^1D)6d(^2S)$ with term values of 3.70 eV and 2.34 eV for the states, respectively, with respect to the $4p^{-2}(^1D)$ ionization threshold at 40.17 eV [30]. By assuming that the $4p\pi^{-2}nd\lambda$ states also mix strongly to the $4s\sigma^{-1}$ state, the narrow lines of groups *F* and *G* in the photoelectron spectrum of HBr are assigned to the final ionic states $4p\pi^{-2}(^1\Delta)5d\delta(^2\Sigma^+)$ and $4p\pi^{-2}(^1\Delta)6d\delta(^2\Sigma^+)$, respectively, based on their term values of 3.45 eV and 2.30 eV relative to the $4p\pi^{-2}(^1\Delta)$ threshold with a binding energy of 33.94 eV. The lines at the higher-binding-energy side of groups *F* and *G* are probably due to vibrational excitations. The narrow lines of groups *A*, *C*, and *D* are closely related to the resonant Auger spectra taken at the $3d^{-1}5s\sigma$ resonances and will be discussed at the end of this section.

A least-squares fit analysis of the $4s\sigma^{-1}$ photoelectron spectrum of HBr was also performed. The results of this analysis are summarized in Table I and Fig. 1. The narrow lines are described by one narrow Gaussian profile; it turned out that all well separated lines exhibit total linewidths between 30 and 35 meV, which are due to the total experimental contribution. The broad lines, which are due to transitions to the dissociative states, were described with one or several broad Gaussians; more than one Gaussian were applied to asymmetric lines, e.g., line *B*. The broad part of the spectrum, which was described with broad lines, is indicated by the solid subspectrum in Fig. 1 and the fit result of the complex group *C* is shown in the inset of this figure. In particular, group *B* is described by five broad Gaussians (full width at half maximum $\geqslant$165 meV) and a number of narrow Gaussians. The broad Gaussians was assigned to the $4s\sigma^{-1}$ main line and the intensity of all narrow lines were normalized to the sum of the intensity of these five profiles.

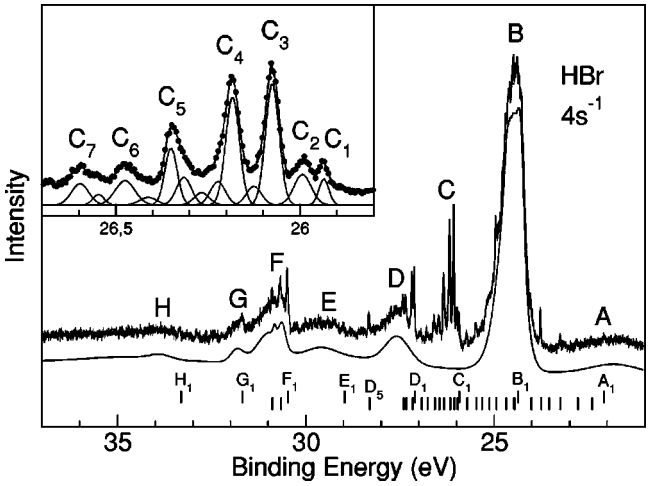

FIG. 1. The photoelectron spectrum of HBr in the inner-valence region taken at 59.4 eV photon energy. The solid subspectrum displays the contributions of the fit result which are due to broad, i.e., dissociative lines. The bars below the spectrum indicate the position of the narrow lines of the ionic final states related to the $4s\sigma^{-1}$ photoelectron line which are summarized in Table I. The bars for the first line of each group are slightly above the other bars and labeled A_1 to H_1. The numbers for the lines increase from right to left. The inset shows the lines of group *C* in detail. The solid line through the data points represents the fit result and the solid subspectra display the different lines in this energy region.

B. The resonant Auger decay at the $3d^{-1}5s\sigma$ resonances

Figure 2(a) shows the Br $4s\sigma^{-1}$ photoelectron spectrum in the binding energy region between 22 and 30 eV, together with the Br $3d_{5/2}^{-1}5s\sigma$ resonant Auger spectra excited at photon energies of $h\nu=73.82$ eV [Fig. 2(c)] and $h\nu=73.90$ eV [Fig. 2(b)]. The corresponding total ion yield spectrum is presented in the inset of Fig. 2. Note that the displayed photoabsorption resonances have recently been reassigned from Br $3d_{5/2}^{-1}4d\pi$ resonances to Br $3d_{5/2}^{-1}5s\sigma$ resonances, based on angle-resolved photoabsorption spectra [23].

The three spectra shown in Fig. 2 are normalized in intensity to broad line *B* (see Fig. 1) of the $4s\sigma^{-1}$ photoelectron spectrum. It can be observed that lines A_4 and A_6, all lines of group C, as well as lines D_1 to D_5 are enhanced in the resonant Auger spectrum taken at the Br $3d_{5/2}^{-1}5s\sigma$ resonances. In addition, two intense narrow lines (I_1 and I_2 at $\cong$24.5 eV) can be observed. Between the binding energies of 26.5 eV and 28.5 eV a considerable increase in the background can be noticed as compared to the $4s\sigma^{-1}$ photoelectron spectrum. (The dotted lines below each spectrum in this energy range indicate the baseline.)

TABLE I. Summary of the energy positions and assignments of the lines observed in the $4s\sigma^{-1}$ photoelectron spectrum, and the resonant Auger spectra of the resonances $3d^{-1}5s\sigma$, $3d^{-1}5p\sigma$, and $3d^{-1}5p\pi$. The lines labeled without an additional subscript are broad and the lines with a subscript are narrow. The assignments indicated with "?" are tentative and discussed in the text. The accuracy of the energy positions of the narrow lines is better than 10 meV. The relative intensities of the narrow lines are given in percent of the intensity of the $4s\sigma^{-1}$ main line (see text) and the accuracies of these intensities are estimated to be on the order of 15% of the relative values.

Label	Binding energy (eV)	Relative intensity	Assignment
A	21.7		$4p\pi^{-2}(^1\Sigma^+)\sigma^*(^2\Sigma^+)$
A_1	22.088	0.107	
A_2	22.428	0.090	
A_3	22.807	0.113	
A_4	23.262	0.215	$4p\pi^{-2}(^3\Sigma^-)5s\sigma(^4\Sigma^-_{1/2})$
A_4	23.295		$4p\pi^{-2}(^3\Sigma^-)5s\sigma(^4\Sigma^-_{3/2})$
A_5	23.562		Vibration of A_4
A_6	23.772	0.689	$4p\pi^{-2}(^3\Sigma^-)5s\sigma(^2\Sigma^-)$
K_1	24.018		$4p\pi^{-2}(^3\Sigma^-)4d\pi(^4\Pi)$?
A_7	24.025	0.176	Vibration of A_6
B_1	24.400	1.135	
B_2	24.497	0.866	
I_1	24.528		$4p\pi^{-2}(^3\Sigma^-)4d\delta(^2\Delta)$?
I_2	24.642		$4p\pi^{-2}(^1\Delta)5s\sigma(^2\Delta)$
B_3	24.698		
K_2	24.762		$4p\pi^{-2}(^3\Sigma^-)4d\pi(^4\Pi)$?
	24.906		Vibration of I_2
B_4	24.957	0.919	
	25.011		Vibration of K_2
B_5	25.177	0.919	
B_6	25.358	0.278	
L_1	25.366		$4p\pi^{-2}(^3\Sigma^-)5p\sigma(^4\Sigma^-)$?
K_3, L_2	25.474		$4p\pi^{-2}(^3\Sigma^-)4d\pi(^2\Phi)$? and/or $4p\pi^{-2}(^3\Sigma^-)5p\sigma(^2\Sigma^-)$?
B_7	25.489	0.516	
K_4	25.602		$4p\pi^{-2}(^3\Sigma^-)5p\pi(^4\Pi)$?
B_8	25.728	0.203	
K_5	25.851		$4p\pi^{-2}(^3\Sigma^-)4d\pi(^2\Pi)$?
C_1	25.935	0.495	$4s\sigma^{-1}(^2\Sigma^+)+4p\pi^{-2}(^1\Sigma)5s\sigma(^2\Sigma^+)$
C_2	25.993	1.002	$4s\sigma^{-1}(^2\Sigma^+)+4p\pi^{-2}(^1\Sigma)5s\sigma(^2\Sigma^+)$
K_6	26.006		$4p\pi^{-2}(^3\Sigma^-)5p\pi(^2\Pi)$?
C_3	26.075	3.162	$4s\sigma^{-1}(^2\Sigma^+)+4p\pi^{-2}(^1\Sigma)5s\sigma(^2\Sigma^+)+4p\pi^{-2}(^3\Sigma^-)5p\pi$ and/or $4p\pi^{-2}(^1\Delta)4d\pi+4p\pi^{-2}5p\sigma$
C_3	26.125	0.529	
C_4	26.183	2.823	$4s\sigma^{-1}(^2\Sigma^+)+4p\pi^{-2}(^1\Sigma)5s\sigma(^2\Sigma^+)+4p\pi^{-2}(^3\Sigma^-)5p\pi$ and/or $4p\pi^{-2}(^1\Delta)4d\pi+4p\pi^{-2}5p\sigma$
C_4	26.223	0.661	
C_4	26.267	0.348	
C_5	26.315	0.780	
C_5	26.350	1.342	$4s\sigma^{-1}(^2\Sigma^+)+4p\pi^{-2}(^1\Sigma)5s\sigma(^2\Sigma^+)+4p\pi^{-2}(^3\Sigma^-)5p\pi$ and/or $4p\pi^{-2}(^1\Delta)4d\pi+4p\pi^{-2}5p\sigma$
C_6	26.412	0.243	
C_6	26.475	0.912	$4s\sigma^{-1}(^2\Sigma^+)+4p\pi^{-2}(^1\Sigma)5s\sigma(^2\Sigma^+)$

TABLE I. (*Continued*).

Label	Binding energy (eV)	Relative intensity	Assignment
C_7	26.547	0.224	
C_7	26.597	0.697	$4s\sigma^{-1}(^2\Sigma^+)+4p\pi^{-2}(^1\Sigma)5s\sigma(^2\Sigma^+)$
L_3	26.706		$4p\pi^{-2}(^1\Delta)5p\sigma(^2\Delta)$
C_8	26.791	0.238	
L_4	26.938		Vibration of L_3
C_9	26.955	0.096	
L_4	26.994		
D_1	27.128	1.161	$4s\sigma^{-1}(^2\Sigma^+)+4p\pi^{-2}4d\pi$
D_2	27.185	1.125	$4s\sigma^{-1}(^2\Sigma^+)+4p\pi^{-2}4d\pi$
D_3	27.350	0.556	Vibration of D_3
D_4	27.423	0.358	Vibration of D_4
L_5	27.910		$4p\pi^{-2}(^1\Sigma^+)5p\sigma(^2\Sigma^+)$
L_6	28.094		Vibration of L_5
K_7	26.843		$4p\pi^{-2}(^1\Delta)5p\pi(^2\Phi)$?
K_8	27.027		$4p\pi^{-2}(^1\Delta)5p\pi(^2\Pi)$?
D_5	28.322	0.407	$4p\pi^{-2}(^1\Sigma^+)5p\pi(^2\Pi)$
K_9	28.514		Partly vibration of D_5
E	29.0		$4p\sigma^{-1}4p\pi^{-1}(^{1,3}\Pi)5p\pi(^2\Sigma^+)$?
M_1	30.270		$4p\pi^{-2}6p$ shake-up
M_2	30.490		$4p\pi^{-2}6p$ shake-up
F_1	30.494	1.279	$4p\pi^{-2}(^1\Delta)5d\delta(^2\Sigma^+)$
F_2	30.689	0.548	Vibration to F_1
M_3	30.882		$4p\pi^{-2}6p$ shake-up
F_3	30.901	0.346	Vibration to F_1
M_4	31.526		$4p\pi^{-2}6p$ shake-up
M_5	31.638		$4p\pi^{-2}6p$ shake-up
G_1	31.694	0.376	$4p\pi^{-2}(^1\Delta)6d\delta(^2\Sigma^+)$
H_1	33.355	0.158	
H	33.85		

The main difference between the two resonant Auger spectra is that all enhanced lines are more intense subsequent to an excitation of $h\nu=73.82$ eV [Fig. 2(c)] as compared to $h\nu=73.90$ eV [Fig. 2(b)]. This can be understood by the higher cross section for the photon energy of $h\nu=73.82$ eV (see inset). Lines A_4 and A_6, however, are exceptions. Their increase in Fig. 2(c) as compared to Fig. 2(b) does not scale with the cross section of the excitation process. In particular, the intensity ratio between these lines changes considerably. This is in contradiction to a two-step model with the excited electron being considered as a spectator during the Auger decay, and can probably be explained by interference effects between the 4s photoionization and the resonant Auger channels [35,36] or by electronic lifetime interference between two resonance channels related to the resonant Auger decay via two intermediate states [37]. However, this is a subject beyond the scope of the present work.

C. Discussion

By assuming the excited electron to be a spectator during the decay, the most intense narrow lines in the Br $3d^{-1}5s\sigma$ resonant Auger decay spectra are expected to be due to transitions to the $4p\pi^{-2}5s\sigma$ configuration. From the normal Auger spectrum it was derived that the $4p\pi^{-2}$ configuration splits into the parent states $^3\Sigma_0^-$, $^3\Sigma_1^-$, $^1\Delta$, and $^1\Sigma^+$ with a splitting of 55(10) meV, 1359(10) meV, and 2624(10) meV between the $^3\Sigma_0^-$ and $^3\Sigma_1^-$, $^1\Delta$, and $^1\Sigma^+$, respectively [24]. In this way the final states $4p\pi^{-2}(^3\Sigma^-)5s\sigma(^4\Sigma_{3/2}^-,^4\Sigma_{1/2}^-,^2\Sigma^-)$, $4p\pi^{-2}(^1\Delta)5s\sigma(^2\Delta)$, and $4p\pi^{-2}(^1\Sigma^+)5s\sigma(^2\Sigma^+)$ can be derived for the $4p\pi^{-2}5s\sigma$ configuration. As already observed in the Cl $2p^{-1}4s\sigma$ resonant Auger spectrum in HCl [16], the energetic splitting of the final states should be dominated by the splitting of the parent states, which is indicated with the vertical-bar diagram in the upper right corner of Fig. 2. From this it can readily be derived that the lines A_4 and A_6 are associated with the $^3\Sigma^-$ parent state, I_1 and I_2 with the $^1\Delta$ parent state, and the enhancement of all lines of group C with the $^1\Sigma^+$ parent state.

As a consequence of these considerations, lines A_4 and A_6 are assigned to transitions to $4p\pi^{-2}(^3\Sigma^-)5s\sigma(^4\Sigma^-)$ and $4p\pi^{-2}(^3\Sigma^-)5s\sigma(^2\Sigma^-)$, respectively. The assignment for line A_4 is supported by a small splitting of $\cong 30$ meV of the $^4\Sigma^-$ state into the components $^4\Sigma_{3/2}^-$ and $^4\Sigma_{1/2}^-$ which is due to spin-orbit interaction; this splitting clearly reveals this state to be of quartet character. This result also agrees with

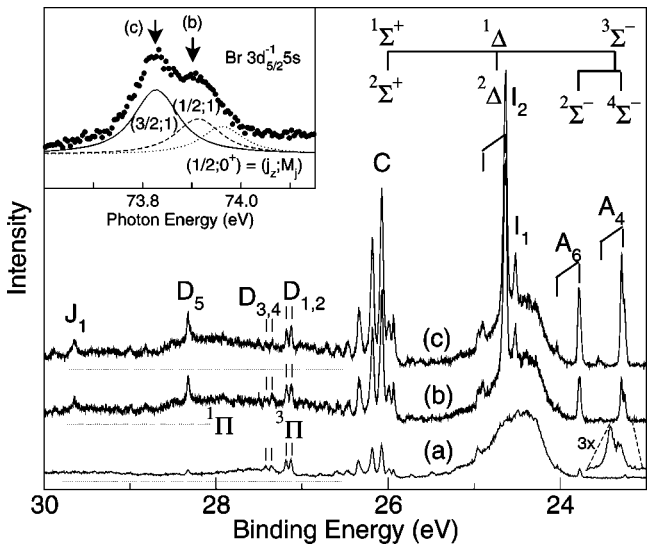

FIG. 2. The $4s^{-1}$ photoelectron spectrum taken at 59.4 eV (a) as well as the $3d^{-1}5s\sigma$ resonant Auger decay spectra taken at excitation energies of 73.82 eV (b) and 73.90 eV (c). The vertical bar diagram in the upper right corner indicates the splitting of the $4p\pi^{-2}$ parent states and the assignment of the symmetry of the final states of the Auger decay. The dotted lines below each spectrum in the higher-binding-energy region indicate the baselines. At low binding energies below spectrum (b) line A_4 is shown with an energy scale stretched by a factor of 3, revealing clearly two components. Inset: Total ion yield spectrum in the $3d^{-1}_{5/2}5s\sigma$ region including the resonances $3d^{-1}_{5/2,3/2}5s\sigma(M_j=1)$, $3d^{-1}_{5/2,1/2}5s\sigma(M_j=1)$, and $3d^{-1}_{5/2,1/2}5s\sigma(M_j=0^+)$. The arrows indicated with (b) and (c) in the inset show the excitation energies for spectra (b) and (c) in the main figure.

the splitting of 55(10) meV of the $4p\pi^{-2}(^3\Sigma^-)$ final state of the normal Auger decay into the components $^3\Sigma^-_0$ and $^3\Sigma^-_1$ obtained from the fit [24] and calculations [38].

The intense line I_2 is assigned to the transition from the intermediate state $3d^{-1}5s\sigma$ to the $4p\pi^{-2}(^1\Delta)5s\sigma(^2\Delta)$ final state. In principle, this final state splits into the components $^2\Delta_{3/2}$ and $^2\Delta_{5/2}$, however, for this splitting we expect a value similar to that obtained for the $^4\Sigma^-$ states. We, therefore, rule out the assignment of the lines I_1 and I_2 to the $^2\Delta_{3/2}$ and $^2\Delta_{5/2}$ components of the state $^2\Delta$, since the observed splitting of $\cong$115 meV is much larger. Instead we suggest a final-state mixing between the final state $4p\pi^{-2}(^1\Delta)5s\sigma(^2\Delta)$ and another final state of $^2\Delta$ symmetry, which is probably $4p\pi^{-2}(^3\Sigma^-)4d\delta(^2\Delta)$.

In the resonant Auger spectrum taken at the $3d^{-1}5s\sigma$ resonances, all lines of group *C* in the $4s\sigma^{-1}$ photoelectron spectrum are strongly enhanced. These lines are all predominantly of $^2\Sigma^+$ symmetry since these are strong in the direct photoelectron spectrum. This is in full agreement with the observation that the intensity of these lines is strongly enhanced by an Auger decay to the final state $4p\pi^{-2}(^1\Sigma^+)5s\sigma(^2\Sigma^+)$. It is well known [16] that the corresponding energy region in HCl shows a strong mixing of different $^2\Sigma^+$ final states, resulting in a spectral feature similar to that observed in HBr. It should be pointed out that an adequate description of these lines in terms of one strong vibrational progression is not possible since the energetic distances between the lines are irregular. A Franck-Condon analysis based on the assumption of two or three transitions with a strong vibrational progression for each transition did not result in a satisfactory description of the spectrum as well. We, therefore, suggest the lines of group C to be predominantly due to a strong mixing between a number of $^2\Sigma^+$ final states which are stable with respect to dissociation, namely, $4s\sigma^{-1}$, $4p\pi^{-2}(^1\Sigma^+)5s\sigma(^2\Sigma^+)$, $4p\pi^{-2}(^1\Sigma^+)6s\sigma(^2\Sigma^+)$, $4p\pi^{-2}(^1\Sigma^+)5p\sigma(^2\Sigma^+)$, $4p\pi^{-2}(^1\Sigma^+)4d\sigma(^2\Sigma^+)$, and $4p\pi^{-2}(^1\Delta^+)4d\delta(^2\Sigma^+)$. From the present spectra we can directly conclude that the configuration $4s\sigma^{-1}(^2\Sigma^+)$ contributes to the lines of group *C* since these are present in the photoelectron spectrum and the intensity can only be caused by transitions to this configuration. We can also conclude that all lines must have strong contributions of the final state $4p\pi^{-2}(^1\Sigma^+)5s\sigma(^2\Sigma^+)$ since these are strongly enhanced in the Br $3d^{-1}5s\sigma$ resonant Auger decay. We also found a slight enhancement of the lines C_3, C_4, and C_5 in the resonant Auger spectra taken at the $3d^{-1}5p\sigma$ and $3d^{-1}5p\pi$ resonances, which underlines some contribution of the final state $4p\pi^{-2}(^1\Sigma^+)5p\sigma(^2\Sigma^+)$ as well as the $4p\pi^{-2}5p\pi$ to these lines. However, a mixing of only these four states is not sufficient to explain the large number of lines of group *C*. We have to conclude that other states in addition to the abovementioned states contribute to the mixing, although we cannot prove their contributions based on the experimental findings.

The enhanced background in the $3d^{-1}5s\sigma$ resonant Auger spectra in the energy region between 25.5 eV and 27.5 eV is assigned to transitions to the dissociative final states $4p\sigma^{-1}4p\pi^{-1}(^1\Pi)5s\sigma(^2\Pi)$ and $4p\sigma^{-1}4p\pi^{-1}(^3\Pi)5s\sigma(^{2,4}\Pi)$ which are expected to be $\cong$2 eV and $\cong$1 eV above the $4p\pi^{-2}(^1\Sigma^+)5s\sigma(^2\Sigma^+)$ final state, respectively [24].

The lines D_1 to D_4 show essentially the same intensity in the $4s^{-1}$ photoelectron and the $3d^{-1}5s\sigma$ resonant Auger spectrum, giving rise to the assumption that these possess only minor contributions from the $4p\pi^{-2}5s\sigma$ configuration. The weak line D_5, however, is clearly enhanced and an additional line J_1 can be observed in the resonant Auger spectrum. According to the findings in the $3d^{-1}5p\pi$ resonant Auger spectrum, line D_5 is assigned to transitions to $4p\pi^{-2}(^1\Sigma^+)5p\pi(^2\Pi)$ (see below) and its presence in the $4s\sigma^{-1}$ photoelectron spectrum can be explained by spin-orbit interaction in the final ionic state, and this clearly shows that configurations with $^2\Sigma^+$ symmetry are not sufficient for a complete description of the $4s^{-1}$ photoelectron spectrum. This also holds for the lines A_4 and A_6, which are assigned to transitions to states of $^4\Sigma^-$ and $^2\Sigma^-$ symmetries, respectively, and are present in both, the photoelectron spectrum and the resonant Auger spectrum. Spin-orbit interaction may also explain the appearance of a number of weak lines, e.g., A_1 to A_3 by assuming that their final states are mainly of $\Sigma\Lambda$ symmetries different from $^2\Sigma^+$. The intensity of the satellite lines with a symmetry different from $^2\Sigma^+$ in the $4s\sigma^{-1}$ photoemission spectrum can be due to shake-up states of the $4p\pi^{-1}$ photoemission as well. However, it is

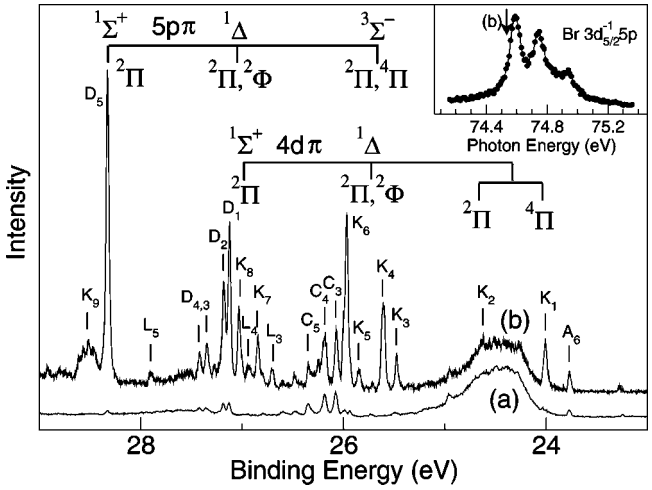

FIG. 3. The $4s^{-1}$ photoelectron spectrum taken at 59.4 eV (a) and the resonant Auger decay spectrum of a $3d_{5/2,5/2}^{-1}5p\pi$ resonance, taken at a photon energy of 74.53 eV (b). The vertical-bar diagrams indicates the splittings of the $4p\pi^{-2}$ parent states for the configurations $4p\pi^{-2}5p\pi$ and $4p\pi^{-2}4d\pi$. Inset: Total ion yield spectrum in the $3d_{5/2}^{-1}5p$ region. The arrow indicated with (b) in the inset denotes the photon energy for the excitation process.

known for the $4s^{-1}$ satellite lines in the isoelectronic atom Kr that 75% of the intensity is due to spin-orbit interaction and only 20% is due to shake-up processes [30]. Therefore we expect spin-orbit interaction to be dominant in the $4s\sigma^{-1}$ photoemission spectrum of HBr.

IV. THE RESONANT AUGER SPECTRA AT THE $3d^{-1}5p$ RESONANCES

A. The spectra taken at the $3d^{-1}5p\pi$ resonances

Figure 3(b) displays the resonant Auger spectrum measured at $h\nu=74.53$ eV together with the $4s\sigma^{-1}$ photoelectron spectrum [Fig. 3(a)]. At a photon energy of 74.53 eV the resonance is of rather pure $3d_{5/2,5/2}^{-1}5p\pi$ character so that it can be assumed that other resonant Auger decays contribute only in a minor way to the spectrum; the weak lines indicated as L_3, L_4, and L_5 are the strongest ones of the $3d^{-1}5p\sigma$ resonant Auger decay (see discussion below and Fig. 4).

Apparently, the lines D_1 to D_5, which are weak in the $4s\sigma^{-1}$ photoelectron spectrum, are strongly enhanced. This is also true to some degree for the lines C_3 to C_5 and A_6. In addition to the enhanced lines, there are nine lines, which cannot be observed in the $4s\sigma^{-1}$ photoelectron spectrum; these are labeled to K_1 to K_9.

The energetic spread of the enhanced lines is about 4.5 eV, which is much larger than that of the resonant Auger decay spectrum taken at the $3d^{-1}5s\sigma$ resonance and the splitting of the $4p\pi^{-2}$ parent states $^1\Sigma^+$, $^1\Delta$, and $^3\Sigma^-$. In addition, the intense lines can be divided into four groups as can be seen by the vertical-bar diagrams in the upper part of Fig. 3. All lines are present with similar intensity ratios in all $3d^{-1}5p\pi$ resonant Auger spectra independent of the excitation energies [compare, e.g., Fig. 4(c)]. Therefore, an accidental overlap with a previously unobserved resonance at

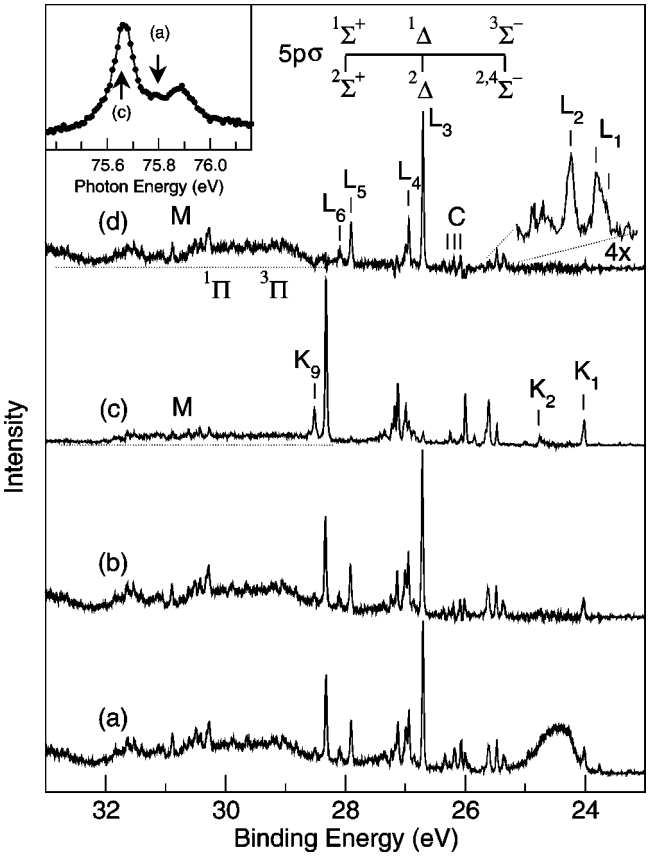

FIG. 4. The resonant Auger spectrum subsequent to excitation into the states $3d_{3/2,1/2}^{-1}5p\sigma$ and $3d_{3/2,1/2}^{-1}5p\pi$ using a photon energy $h\nu=75.80$ eV (a) and the same spectrum after subtracting the contributions of the $4s\sigma^{-1}$ photoelectron lines (b). (c): The resonant Auger spectrum of the $3d_{3/2,3/2}^{-1}5p\pi$ resonance at $h\nu=75.66$ eV after subtraction of the contributions of the $4s\sigma^{-1}$ photoelectron lines. (d): Spectrum (b) after subtracting of the contributions of the $3d^{-1}5p\pi$ resonant Auger lines, i.e., a "pure" $3d^{-1}5p\sigma$ resonant Auger spectrum. The vertical-bar diagram indicates the splitting of the parent states for the $4p\pi^{-2}5p\sigma$ configuration. The dotted lines below spectra (c) and (d) indicate the baseline. At low binding energies above spectrum (d) lines L_1 and L_2 are shown with an energy scale stretched by a factor of 4, revealing clearly two components for L_1. Inset: Total ion yield spectrum of HBr in the energy region between 75.36 eV and 76.16 eV. The arrows marked with (a) and (c) show the excitation energies for the resonant Auger spectra (a) and (c).

one energy in the photoabsorption spectrum can be excluded. For these findings two different explanations are possible. As the first possibility, the observed lines can be due to the resonant Auger decay of a previously unobserved resonance in the photoabsorption spectrum which is at almost identical excitation energies (with differences of less than 10 or 15 meV) as the $3d^{-1}5p\pi$ resonances in all five ligand-field split components. From the results of the angle-resolved photoabsorption spectra [23], we have to conclude that such possible additional resonances must have π symmetry in the Rydberg orbital, i.e., the only possible resonance in this energy region would be $3d^{-1}4d\pi$. Although such accidentally identical excitation energies seem to be unlikely, we cannot

exclude them. Note that nearly degenerate resonances may not remain clean but get mixed through the configuration interaction in the excited state. In addition, we introduce—as a second option—a final-state configuration interaction between the $4p\pi^{-2}5p\pi$ states with states of the same $\Sigma\Lambda$ symmetry, namely, $4p\pi^{-2}4d\pi$, giving rise to two sets of parent states as indicated by the vertical-bar diagrams.

The effect of the mixing can be described using a simple picture that introduces, instead of the full configuration interaction approach, an expansion for the Rydberg orbital in terms of the $5p\pi$ and $4d\pi$ orbitals. By using atomic Br orbitals as a basis set, the angle Θ between the site of the highest probability density for the electron, the Br nucleus, and the H nucleus is 90° for the Br $5p\pi$ and 45° as well as 135° for the Br $4d\pi$ orbital in the ground-state electron configuration of HBr. However, the $5p\pi$ Rydberg electron in a $3d^{-1}$ state experiences a nonspherical charge distribution caused by the molecular core so that Θ can be assumed to be different from 90°. At such angles of Θ different from 90° the Rydberg electron can be described by linear combinations of the $nl\lambda$ Rydberg orbitals of atomic bromine. In order to simplify the discussion we restrict the basis set to the atomic orbitals Br $5p\pi$, $|5\mathrm{p}\pi(\mathrm{Br})\rangle$, and Br $4\mathrm{d}\pi$, $|4\mathrm{d}\pi(\mathrm{Br})\rangle$. In this case the $5p\pi$ and the $4d\pi$ Rydberg orbitals in the $3d^{-1}nl\lambda$ states can be described as $|5p\pi(\mathrm{HBr}\ 3d^{-1})\rangle = \alpha|5p\pi(\mathrm{Br})\rangle + \beta|4d\pi(\mathrm{Br})\rangle$ and $|4d\pi(\mathrm{HBr}\ 3d^{-1})\rangle = \beta|5p\pi(\mathrm{Br})\rangle - \alpha|4d\pi(\mathrm{Br})\rangle$. The two excited states, one with a pronounced $5p\pi$ character and the other with a pronounced $4d\pi$ character may get populated in photoexcitation. If only the dipole transition to $5p$ is allowed, as it is in atoms, then the population is determined by the $5p\pi$ character of the states. As a consequence, the photoabsorption spectra display the features of the transitions to the $5p\pi$ only, even though the excited state itself has some $4d\pi$ character ($\beta \neq 0$). The decay spectrum instead is sensitive also to the $4d\pi$ character of the excited state. The resonant Auger decay rearranges the charge distribution of the molecular core, leading to a different angle for Θ in the $4p\pi^{-2}5p\pi$ states. As a consequence, different linear combinations of the atomic bromine orbitals $5p\pi$ and $4d\pi$ are necessary to describe the Rydberg electron in the final state of the resonant Auger process, i.e., $|5p\pi(\mathrm{HBr}4p^{-2})\rangle = \gamma|5p\pi(\mathrm{Br})\rangle + \delta|4d\pi(\mathrm{Br})\rangle$ and $|4d\pi(\mathrm{HBr}\ 4p^{-2})\rangle = \delta|5p\pi(\mathrm{Br})\rangle - \gamma|4d\pi(\mathrm{Br})\rangle$ with $\alpha \neq \gamma$ and $\beta \neq \delta$.

By assuming the Rydberg electron to be a spectator during the Auger decay in the core, the population of the $4p\pi^{-2}4d\pi$ configuration can be understood. Such states [described above with Rydberg electron $|4d\pi(\mathrm{HBr}\ 4p^{-2})\rangle$] get populated via the transitions from both excited states, from at with $|5p\pi(\mathrm{HBr}\ 3d^{-1})\rangle$ Rydberg electron and from at with $|4d\pi(\mathrm{HBr}\ 3d^{-1})\rangle$. In this simple picture, which completely omits the coupling between the spectator and the core, the mixing coefficients play the most prominent role when estimating the population. They, furthermore, are sensitive to the changes in charge distribution that results from the angular rearrangement during the excitation/Auger decay. If $\beta \cong 0$ but $\delta \neq 0$, the final ionic state configuration interaction is the effect which feeds the states with pronounced $4p\pi^{-2}4d\pi$ character.

From the configurations $4p\pi^{-2}nl\pi$, one can derive the final states $4p\pi^{-2}(^1\Sigma^+)nl\pi(^2\Pi)$, $4p\pi^{-2}(^1\Delta)nl\pi(^2\Pi,^2\Phi)$, and $4p\pi^{-2}(^3\Sigma^-)nl\pi(^2\Pi,^4\Pi)$, none of them having a $^2\Sigma^+$ symmetry. Since a number of the lines in the $3d^{-1}5p\pi$ resonant Auger spectrum are only strongly enhanced as compared to the $4s^{-1}$ photoelectron spectrum, it becomes once again obvious that there is a strong spin-orbit interaction between states of different $\Sigma\Lambda$ symmetry. It also allows us to give a more detailed assignment of the $4s^{-1}$ photoelectron spectrum.

The strongest line in the $3d^{-1}5p\pi$ resonant Auger spectrum, D_5, is assigned to a transition to the state $4p\pi^{-2}(^1\Sigma^+)5p\pi(^2\Pi)$ by assuming a spectator behavior for the excited Rydberg electron. Its presence in the $4s^{-1}$ photoelectron spectrum is due to a spin-orbit interaction. Note that in the energy region under discussion there is a strong mixing between different states of the same $\Sigma\Lambda$ symmetry due to configuration interaction as well as between states of different $\Sigma\Lambda$ symmetries due to spin-orbit interaction. As a consequence, all assignments given for the $3d^{-1}5p\pi$ resonant Auger spectrum indicate only the assumed main contribution of a given line. The lines D_1 to D_4 are more intense in the $4s^{-1}$ photoelectron spectrum than the line D_5 and these are less enhanced in the $3d^{-1}5p\pi$ resonant Auger spectrum than some other lines, e.g., D_5. Both findings agree with the assumption that final states of these lines have a stronger contribution of the $\Sigma\Lambda$-state $4p\pi^{-2}(^1\Sigma^+)4d\pi(^2\Pi)$ as compared to line D_5, if one assumes that the mixing between $4p\pi^{-2}4d$ and $4s^{-1}$ is as strong as it is observed for Kr [30]. The energetic splitting of $\cong$60 meV and almost constant intensity ratios between D_1 and D_3 as well as D_2 and D_4 can be explained with two electronic final states, lines D_1 and D_2, and a vibrational fine structure, lines D_3 and D_4. Lines L_3 and L_4 can be related to the resonant Auger spectra at the $3d^{-1}5p\sigma$ resonance (see below). As a consequence the final states of the lines K_8 and K_7 are most probably of the $4p\pi^{-2}(^1\Delta)5p\pi(^2\Pi)$ and $4p\pi^{-2}(^1\Delta)5p\pi(^2\Phi)$ character, respectively, using Hund's rules for the assignment.

The enhancement of the lines C_3 to C_5 shows that these final states also have some $4p\pi^{-2}4d\pi$ and/or $4p\pi^{-2}5p\pi$ contributions in addition to the already stated contributions $4s^{-1}$ and $4p\pi^{-2}(^1\Sigma^+)5s\sigma(^2\Sigma)$. Lines K_3 to K_6 are probably related to the states $4p\pi^{-2}(^3\Sigma^-)5p\pi(^2\Pi,^4\Pi)$ and $4p\pi^{-2}(^1\Delta)4d\pi(^2\Pi,^2\Phi)$. According to the fact that the lines K_4 and K_6 are stronger than the lines K_3 and K_5 and according to the expected binding-energy orders based on Hund's rules ($E_{\mathrm{bin}}[4p\pi^{-2}(^3\Sigma^-)5p\pi(^2\Pi)] > E_{\mathrm{bin}}[4p\pi^{-2}(^3\Sigma^-)5p\pi(^4\Pi)]$; $E_{\mathrm{bin}}[4p\pi^{-2}(^1\Delta)4d\pi(^2\Pi)] > E_{\mathrm{bin}}[4p\pi^{-2}(^1\Delta)4d\pi(^2\Phi)]$), we slightly prefer the assignment of K_6 to K_3 to transitions to $4p\pi^{-2}(^3\Sigma^-)5p\pi(^2\Pi)$, $4p\pi^{-2}(^1\Delta)4d\pi(^2\Pi)$, $4p\pi^{-2}(^3\Sigma^-)5p\pi(^4\Pi)$, and $4p\pi^{-2}(^1\Delta)4d\pi(^2\Phi)$, respectively.

Lines K_2 and K_1 are assigned to transitions to $4p\pi^{-2}(^3\Sigma^-)4d\pi(^2\Pi)$ and $4p\pi^{-2}(^3\Sigma^-)4d\pi(^4\Pi)$, respectively. Line K_9 consists of at least four lines. These lines can

only be assigned to a minor part to the vibrational fine structure of the line D_5 since the structure is almost identical in HBr and DBr (not shown here), i.e., no isotopic shift or change in the intensity ratio can be observed as expected for vibrational excitations. In addition, this part of the spectrum looks different after an excitation to a $3d_{3/2}^{-1}5p\pi$ Rydberg state [see Fig. 4(c) as compared to Fig. 3(b) which shows a $3d_{5/2}^{-1}5p\pi$ Rydberg state].

B. The spectra taken at the $3d^{-1}5p\sigma$ resonances

No well separated $3d^{-1}5p\sigma$ resonance can be found in the photoabsorption spectrum of HBr below the Br $3d^{-1}$ ionization threshold. Because of this, no pure resonant Auger spectrum at the Br $3d^{-1}5p\sigma$ resonances can be presented contrary to the $3d^{-1}5s\sigma$ and $3d^{-1}5p\pi$ resonances, which are in some cases well separated. Figure 4(a) shows a spectrum measured at a photon energy of $h\nu=75.80$ eV containing the resonant Auger decays of the $3d^{-1}5p\sigma$ and $3d^{-1}5p\pi$ resonance states as well as the Br $4s^{-1}$ photoelectron lines. In order to present the $3d^{-1}5p\sigma$ resonant Auger decay lines we performed a procedure as follows. From the spectrum shown in Fig. 4(a) a weighted $4s^{-1}$ photoelectron spectrum (normalized to line B) was subtracted in order to remove all contributions typical for the Br $4s^{-1}$ photoelectron spectrum. The result is shown in Fig. 4(b). A similar procedure was performed for the resonant Auger spectrum taken at 75.66 eV; at this photon energy a well separated $3d_{3/2,3/2}^{-1}5p\pi$ resonance is present in the photoabsorption spectrum. The obtained ''pure'' $3d^{-1}5p\pi$ resonant Auger spectrum is presented in Fig. 4(c). By subtracting a weighted ''pure'' $3d^{-1}5p\pi$ resonant Auger spectrum from Fig. 4(b), a ''pure'' $3d^{-1}5p\sigma$ spectrum is obtained and shown in Fig. 4(d). It should be noted that lines D_5 and K_1, which are the most intense, well separated lines for a $3d^{-1}5p\pi$ resonant Auger spectrum, have almost vanished in Fig. 4(d). Thus, we can consider the spectrum in Fig. 4(d) as a rather pure $3d^{-1}5p\sigma$ resonant Auger spectrum.

In the spectrum of Fig. 4(d), lines L_1 to L_6, in addition to the lines C_1 to C_3, can be found. Since the contributions of the $4s^{-1}$ photoelectron spectrum are eliminated, the presence of the lines C_1 to C_3 in the spectrum is due to an enhancement subsequent to a $3d^{-1}5p\sigma$ resonance. This shows that these lines possess also some final-state contributions of the $4p\pi^{-2}5p\sigma$ configuration in addition to all other contributions discussed above.

The lines L_1 to L_6 can readily be understood based on the splitting of the parent states, which is indicated by the vertical-bar diagram. Lines L_1 and L_2 are assigned to transitions to $4p\pi^{-2}(^3\Sigma^-)5p\sigma(^4\Sigma^-)$ and $4p\pi^{-2}(^3\Sigma^-)5p\sigma(^2\Sigma^-)$, respectively. The assignment of L_1 is supported by the splitting into the components $^4\Sigma_{3/2}^-$ and $^4\Sigma_{1/2}^-$ as shown in the inset. The lines L_3 and L_5 are assigned to transitions $4p\pi^{-2}(^1\Delta)5p\sigma(^2\Delta)$ and $4p\pi^{-2}(^1\Sigma^+)5p\sigma(^2\Sigma^+)$, respectively. The lines L_4 and L_6 are $\approx$230 and 180 meV higher in energy than L_3 and L_5, respectively, and are probably due to vibrational excitations.

For binding energies above the transition to the state $4p\pi^{-2}(^1\Sigma^+)5p\sigma(^2\Sigma^+)$ (line L_5) a considerable increase of the background can be observed. This is due to Auger transitions to the final states $4p\sigma^{-1}4p\pi^{-1}(^{1,3}\Pi)\ 5p\sigma(^{2,4}\Pi)$. The symbols $^1\Pi$ and $^3\Pi$ indicate the energy position for the $4p\sigma^{-1}4p\pi^{-1}(^{1,3}\Pi)$ parent states relative to the $4p\pi^{-2}$ parent states [24]. By comparing the relative intensities between the transitions to $4p\pi^{-2}$ and $4p\sigma^{-1}4p\pi^{-1}$ states given in Figs. 4(c) and 4(d) it can be observed that the contributions of the transitions to the $4p\sigma^{-1}4p\pi^{-1}$ final states are stronger in Fig. 4(d). This is not due to the symmetry of the Rydberg orbital [$5p\pi$ in Fig. 4(c) and $5p\sigma$ in Fig. 4(d)], but due to the spatial orientation of the core hole created in the excitation process [17]. In the spectrum of Fig. 4(c) a $3d_{3/2,3/2}^{-1}$ core hole and in Fig. 4(d) a $3d_{3/2,1/2}^{-1}$ core hole is created. The first core hole is mainly oriented perpendicularly to the molecular axis and the second one mostly parallel [22]. Therefore, the first one will show a strong overlap with the $4p\pi$ orbitals and the second one with the $4p\sigma$ orbital which explains the different intensity ratios observed in Figs. 4(c) and 4(d). It should be noted that the large background in Fig. 4(d) might also partly be due to transitions to $4p\sigma^{-1}4p\pi^{-1}(^{1,3}\Pi)5p\pi$ states since in this excitation region the $3d_{3/2,1/2}^{-1}5p\pi$ Rydberg state is also present. Its decay to the $4p\sigma^{-1}4p\pi^{-1}(^{1,3}\Pi)5p\pi$ final state are underestimated in the subtraction procedure. In particular, the presence of the $4p\sigma^{-1}4p\pi^{-1}(^{1,3}\Pi)5p\pi(^2\Sigma^+)$ states can explain the broad line E in the Br $4s\sigma^{-1}$ photoelectron spectrum (Fig. 1).

In addition, there are some weak but narrow lines in the binding-energy region between 30 and 32 eV in Figs. 4(c) and 4(d) (indicated with M). They are due to shake-up satellites to the final-state configurations of the type $4p\pi^{-2}6p$ and well known from the resonant Auger spectra of $3d^{-1}5p$ resonances in Kr [5].

V. VIBRATIONAL FINE STRUCTURES

In the presented spectra only a small number of lines could be identified as vibrational excitations. In addition, for most of the lines identified as vibrational substates the intensity ratio $I(1)/I(0)$, with $I(\nu)$ being the intensity of the vibrational level ν, was much smaller than observed for the corresponding parent states in the normal Auger spectrum [24].

For the final states with excited higher vibrational substates the energy splitting between the transition to the vibrational ground state $\nu=0$ and the first-excited vibrational state $\nu=1$ are summarized in Table II. The splittings for the parent states derived from the normal Auger spectra [24] are also given. It can be seen that the vibrational splittings for the states of the configurations $4p\pi^{-2}5s\sigma$, $4p\pi^{-2}4d\pi$, and $4p\pi^{-2}5p\sigma$ are $\approx$60 meV, 50 meV, and 35 meV above the values of the corresponding parent states, respectively. From this we conclude that the equilibrium distances for these states are smaller than for the $4p\pi^{-2}$ parent states, i.e., the increase in the equilibrium distance as compared to the intermediate state is smaller for the states of the configurations $4p\pi^{-2}5s\sigma$, $4p\pi^{-2}4d\pi$, and $4p\pi^{-2}5p\sigma$ than for the

TABLE II. Summary of the energy splittings, ΔE, in meV between the vibrational ground state $\nu=0$ and the first-excited vibrational state $\nu=1$ for the $4p\pi^{-2}$ parent states and the $4p\pi^{-2}nl\lambda$ configurations. The values for the parent states are derived from the results in Ref. [24].

Configuration	Parent state		
	$^1\Sigma^+$	$^1\Delta$	$^3\Sigma^-$
$4p\pi^{-2}$	151	200	200
$4p\pi^{-2}5s\sigma$		265 ($^2\Delta$)	265 ($^4\Sigma^-$)
			265 ($^2\Sigma^-$)
$4p\pi^{-2}4d\pi$			250 ($^2\Pi$)
$4p\pi^{-2}5p\sigma$	184 ($^2\Delta$)	230 ($^2\Delta$)	

$4p\pi^{-2}$ parent states. This explains the smaller $I(1)/I(0)$ intensity ratio for the transitions to the final states of the resonant Auger decay than for those in the normal Auger decay; note that $I(1)/I(0)\propto(\Delta r)^2$ with Δr being the change in the equilibrium distance between the intermediate and the final state.

The strong correlation between the vibrational energy and the $I(1)/I(0)$ ratio can be seen by comparing the population of the $4p\pi^{-2}5s\sigma$ and the $4p\pi^{-2}5p\sigma$ states. For the states of the first configuration (line A_4, A_6, I_2) the vibrational energies are $\approx$60 meV above the values for the corresponding parent states and the vibrational excitations are very weak. For the states of the second configuration (lines L_3, L_5) the vibrational energies are only $\approx$35 meV above those of the parent states and the $I(1)/I(0)$ ratios are larger.

From these observations we conclude that the low-n Rydberg orbitals in the $4p\pi^{-2}nl\lambda$ configurations of HBr^+ do have some bonding valence character leading to higher vibrational energies and smaller equilibrium distances as compared to the $4p\pi^{-2}$ configurations in HBr^{2+}. This is in particular valid for the lowest Rydberg orbital $5s\sigma$. However, the higher-n Rydberg orbitals of the $4p\pi^{-2}nl\lambda$ configurations are expected to have no bonding character and, consequently, their vibrational energies and equilibrium distances are expected to be similar to the $4p\pi^{-2}$ parent states. Note that the fact of similar equilibrium distances leads to similar $I(1)/I(0)$ ratios.

It should be noted that a similar behavior was observed in HCl [16,17]. In HCl the resonant Auger transitions to the $3p\pi^{-2}4s\sigma$ states show large vibrational energies and little vibrational excitations compared to the $2p^{-1}\rightarrow 3p\pi^{-2}$ normal Auger transitions. For the resonant Auger transitions to the $3p\pi^{-2}4p$ states the vibrational energies and the intensity distributions of the vibrational progression is closer to that of the normal Auger decay. In HCl, the resonant Auger transitions subsequent to a $2p^{-1}\rightarrow 4p$ excitation, which lead to $3p\pi^{-2}4p$ final states, already show a strong vibrational progression [17] contrary to the analogous resonant Auger transitions to the $4p\pi^{-2}5p$ states in HBr. This is probably due to the fact that the vibrational progression for the $2p^{-1}\rightarrow 3p\pi^{-2}$ normal Auger decay in HCl are considerably stronger than the vibrational progressions for the $3d^{-1}\rightarrow 4p\pi^{-2}$ normal Auger decay in HBr as can be seen from the normal Auger spectra [24,39].

VI. SUMMARY AND CONCLUSIONS

The $4s\sigma^{-1}$ photoelectron spectra and the resonant Auger spectra taken at the $3d^{-1}5s\sigma$, $3d^{-1}5p\sigma$, and $3d^{-1}5p\pi$ resonances are presented; all spectra were measured with high photon resolution and spectrometer resolution resulting in total linewidth of $\cong$30 meV. By relating the spectra to each other, assignments for most of the lines were derived. It turned out that mixing of configurations and spin-orbit interaction is important in this energy region, in agreement with the results for the isoelectronic atom krypton. However, vibrational excitations play only a minor role in these spectra. This is due to mixed character of the low-n Rydberg orbitals in the configurations $4p\pi^{-2}nl\lambda$. These orbitals have considerable bonding valence character so that the change in the equilibrium distance between the initial and the final states remains relatively small. More detailed ''state-of-the-art'' calculations are needed for the discussed energy region in HBr. In addition, high-resolution spectra of DBr would allow us to identify vibrational lines with a higher reliability. This would in particular be important to assign a number of less intense narrow lines.

ACKNOWLEDGMENTS

The authors acknowledge the assistance of the staff of MAX-lab during the experiments. Financial support from the Research Council for the Natural Sciences of the Academy of Finland and the Natural Sciences and Engineering Research Council (NSERC) of Canada is acknowledged.

[1] H. Aksela and S. Aksela, J. Electron Spectrosc. Relat. Phenom. **100**, 395 (1999).
[2] M.N. Piancastelli, J. Electron Spectrosc. Relat. Phenom. **107**, 1 (2000).
[3] G.B. Armen, H. Aksela, T. Åberg, and S. Aksela, J. Phys. B **33**, R49 (2000).
[4] H. Aksela, J. Jauhiainen, E. Kukk, E. Nõmmiste, S. Aksela, and J. Tulkki, Phys. Rev. A **53**, 290 (1996).
[5] J. Jauhiainen, H. Aksela, O.P. Sairanen, E. Nõmmiste, and S. Aksela, J. Phys. B **29**, 3385 (1996).
[6] Z.F. Liu, G.M. Bancroft, K.H. Tan, and M. Schachter, Phys. Rev. Lett. **72**, 621 (1994).
[7] O. Björneholm, S. Sundin, S. Svensson, R.R.T. Marinho, A. Naves de Brito, F.Kh. Gel'mukhanov, and H. Ågren, Phys. Rev. Lett. **79**, 3150 (1997).
[8] S. Sundin, F.Kh. Gel'mukhanov, H. Å gren, S.J. Osborne, A. Kikas, O. Björneholm, A. Ausmees, and S. Svensson, Phys. Rev. Lett. **79**, 1451 (1997).
[9] E. Kukk, J.D. Bozek, and N. Berrah, Phys. Rev. A **62**, 032708 (2000).

[10] E. Kukk, G. Snell, J.D. Bozek, W.-T. Cheng, and N. Berrah, Phys. Rev. A **63**, 062702 (2001).
[11] A. De Fanis, K. Nobusada, I. Hjelte, N. Saito, M. Kitajima, M. Okamoto, H. Tanaka, H. Yoshida, A. Hiraya, I. Koyano, M.N. Piancastelli, and K. Ueda, J. Phys. B **35**, L23 (2002).
[12] S. Sundin, S.J. Osborne, A. Ausmees, O. Björneholm, S.L. Sorensen, A. Kikas, and S. Svensson, Phys. Rev. A **56**, 480 (1997).
[13] S. Sundin, F.Kh. Gel'mukhanov, S.J. Osborne, O. Björneholm, A. Ausmees, A. Kikas, S.L. Sorensen, A. Naves de Brito, R.R.T. Marinho, S. Svensson, and H. Ågren, J. Phys. B **30**, 4267 (1997).
[14] S. Sundin, S.L. Sorensen, A. Ausmees, O. Björneholm, I. Hjelte, A. Kikas, and S. Svensson, J. Phys. B **32**, 267 (1999).
[15] G. Öhrwall, S. Sundin, P. Baltzer, and J. Bozek, J. Phys. B **32**, 463 (1999).
[16] E. Kukk, H. Aksela, O.P. Sairanen, E. Nõmmiste, S. Aksela, S.J. Osborne, A. Ausmees, and S. Svensson, Phys. Rev. A **54**, 2121 (1996).
[17] J. Mursu, A. Kivimäki, H. Aksela, and S. Aksela, Phys. Rev. A **58**, R1645 (1998).
[18] Y.F. Hu, G.M. Bancroft, J. Karvonen, E. Nõmmiste, A. Kivimäki, H. Aksela, S. Aksela, and Z.F. Liu, Phys. Rev. A **56**, R3342 (1997).
[19] D.A. Shaw, D. Cvejanović, G.C. King, and F.H. Read, J. Phys. B **17**, 1173 (1984).
[20] Z.F. Liu, G.M. Bancroft, K.H. Tan, and M. Schachter, J. Electron Spectrosc. Relat. Phenom. **67**, 299 (1994).
[21] R. Püttner, M. Domke, K. Schulz, A. Gutiérrez, and G. Kaindl, J. Phys. B **28**, 2425 (1995).
[22] J. Johnson, J.N. Cutler, G.M. Bancroft, Y.-F. Hu, and K.H. Tan, J. Phys. B **30**, 4899 (1997).
[23] R. Püttner, Y.F. Hu, E. Nõmmiste, G.M. Bancroft, and S. Aksela, Phys. Rev. A **65**, 032513 (2002).
[24] R. Püttner, Y.F. Hu, G.M. Bancroft, H. Aksela, E. Nõmmiste, J. Karvonen, A. Kivimäki, and S. Aksela, Phys. Rev. A **59**, 4438 (1999).
[25] A.J. Yencha, A.J. Cormack, R.J. Donovan, K.A. Hopkirk, and G.C. King, Chem. Phys. **238**, 109 (1998).
[26] A.J. Yencha, A.J. Cormack, R.J. Donovan, K.P. Lawley, A. Hopkirk, and G.C. King, Chem. Phys. **238**, 133 (1998).
[27] F. Burmeister, S.L. Sorensen, O. Björneholm, A. Naves de Brito, R.F. Fink, R. Feifel, I. Hjelte, K. Wiesner, A. Giertz, M. Bässler, C. Miron, H. Wang, M.N. Piancastelli, L. Karlsson, and S. Svensson, Phys. Rev. A **65**, 012704 (2002).
[28] L.M. Andersson, F. Burmeister, H.O. Karlsson, and O. Goscinski, Phys. Rev. A **65**, 012705 (2002).
[29] A. Kikas, S.J. Osborne, A. Ausmees, S. Svensson, O.P. Sairanen, and S. Aksela, J. Electron Spectrosc. Relat. Phenom. **77**, 241 (1996).
[30] S. Alitalo, A. Kivimäki, T. Matila, K. Vaarala, H. Aksela, and S. Aksela, J. Electron Spectrosc. Relat. Phenom. **114**, 141 (2001).
[31] M.Y. Adam, M.P. Keane, A. Naves de Brito, N. Correia, P. Balter, B. Wannberg, L. Karlsson, and S. Svensson, J. Electron Spectrosc. Relat. Phenom. **58**, 185 (1992).
[32] Y.F. Hu, Z.F. Liu, R. Püttner, G.M. Bancroft, and S. Aksela, J. Phys. B **32**, 4091 (1999).
[33] M. Hiyama and S. Iwata, Chem. Phys. Lett. **210**, 187 (1993).
[34] A. Banichevich, R. Klotz, and S.D. Payerimhoff, Mol. Phys. **75**, 173 (1992).
[35] S. Alitalo, T. Matila, H. Aksela, A. Kivimäki, M. Jurvansuu, and S. Aksela, Phys. Rev. A **62**, 032710 (2000).
[36] R. Sankari, A. Kivimäki, M. Huttula, T. Matila, H. Aksela, S. Aksela, M. Coreno, G. Turri, R. Camilloni, M. de Simone, and K.C. Prince, Phys. Rev. A **65**, 042702 (2002).
[37] E. Kukk, H. Aksela, A. Kivimäki, J. Jauhiainen, E. Nõmmiste, and S. Aksela, Phys. Rev. A **56**, 1481 (1997).
[38] T. Matila, K. Ellingsen, T. Saue, H. Aksela, and O. Gropen, Phys. Rev. A **61**, 032712 (2000).
[39] R. Püttner, V. Pennanen, T. Matila, A. Kivimäki, M. Jurvansuu, H. Aksela, and S. Aksela, Phys. Rev. A **65**, 042505 (2002).